Reflectance-Based Vicarious Calibration of INSAT-3D Visible and SWIR channels over Little Rann of Kutch

Piyushkumar N. Patel, Hiren Bhatt, R. P. Prajapati, Geetika Tyagi, A. K. Mathur and B. S. Gohil

Calibration Validation Division
Atmospheric & Oceanic Data Validation, Archival and Dissemination Group
Earth,Ocean, Atmosphere, Planetary Sciences and Applications Area
Space Applications Centre
Indian Space Research Organisation
Ahmedabad, INDIA.

Document control sheet

1. Report No.	SAC/EPSA/ADVG/CVD/CAL-VAL/SR/04/2015
2. Publication Date	May, 2015
3. Title	Reflectance-Based Vicarious Calibration of INSAT-3D on High-Reflectance Ground Target
4. Type of Report	Scientific
5. Number of pages	37
6. Number of references	18
7. Authors	Piyushkumar N Patel, Hiren Bhatt, R P Prajapati, Geetika Tyagi, A K Mathur and B S Gohil
8. Originating unit	CVD/ADVG/EPSA
9. Abstract	This document describes the vicarious calibration of VIS and SWIR channels of INSAT-3D imager and VIS channel of INSAT-3D sounder carried out during five clear sky days in February-March 2015. Top of the atmosphere radiances over Little Rann of Kutchh were simulated using 6S radiative transfer code and matches well with the INSAT-3D observed radiances.
10. Key Words	Vicarious Calibration, INSAT-3D, Visible channel, SWIR channel, Radiance, Reflectance.
11. Security classification	Unrestricted
12. Distribution statement	Among all concerned

Contents

Figures

Tables

Abstract

Looking towards the advancements and popularity of remote sensing and an ever increasing need for the development of a variety of new and complex satellite sensors, it has become even more essential to continually upgrade the ability to provide absolute calibration of sensors.The calibration of satellite sensors is a primary action for the precise retrieval and validation of geophysical products derived from satellite data. This article presents a simple procedure to carry out post-lunch calibration for visible (IMG-VIS) (0.55-0.75 μm) and short-wave infrared (IMG-SWIR) (1.55-1.70 μm) channels of INSAT-3D imager and visible channel (0.645-0.745 μm)of INSAT-3D sounder (SND-VIS) over land site (Little Rann of Kutch (ROK), Gujarat) on five clear-sky days (17th February 2015, 20th February 2015, 05th March 2015, 17th March 2015 and 20th March 2015). This activity is carried out for the explanation of errors or undetermined post-launch changes in sensor spectral response. The surface reflectance and atmospheric properties have been measured during sensor image acquisition period. These data sets were input to the 6S radiative transfer (RT) code along with spectral response function (SRF) of each filter to compute the top of the atmosphere (TOA) spectral radiance for VIS and SWIR bands. The uncertainties due to spatial variability of surface reflectance and due to variation of aerosol types in vicarious calibration coefficient were computed for the INSAT-3D. MODIS Bidirectional Reflectance Distribution Function (BRDF) product was also used to account for the effect of surface anisotropy on radiance at TOA.

The results show that there is no indication of change in calibration coefficients for VIS and SWIR bands of INSAT-3D imager and VIS band of INSAT-3D sounder over Little ROK for these five days. Analysis shows that for clear sky days, the INSAT-3D overestimates TOA radiance by 0.38%, 0.18% and 0.13% for IMG-VIS, IMG-SWIR and SND-VIS, respectively, compared to 6S simulated radiance. In the inverse mode, the 6S corrected surface reflectance was closer to ground measured surface reflectance for these bands. The result illustrate that pre-flight calibration of INSAT-3D imager is consistent with in-flight performance of the instruments.

1. Introduction

The advancements and popularity of satellite remote sensing data usage for societal benefits not only requires the development of new and complex satellites, but also to improve the quality of the satellite sensor and data products. Therefore, it has become even more essential to continually upgrade the ability to provide calibration of sensors. Vicarious calibration provides a method for the absolute calibration of satellite sensors using reference to precise measurements of spectral reflectance from the ground instruments. This absolute calibration produces the calibration coefficients that can be replace with pre-launch laboratory derived coefficients. The calibration procedure includes on-board calibration (Bruegge et al., 1993) and radiometric calibration prior to launch (Bruegge et al., 1998) but where the on-board calibration facility does not exist for the requirement of absolute calibration, in that case a post-launch calibration needs to compensate the degradation of the satellite sensor (Rao, 2001). A vicarious calibration is broadly adopted technique to monitor the radiometric performance of satellite sensor, which involves the computation of uncertainties in the calibration coefficients to correct the radiometric response of the satellite sensor (Thome et al., 1998). Vicarious calibration is performing with radiance simulation using ground measured reflectance and atmospheric parameters in the homogenous conditions to those at the satellite level.

INSAT-3D is an advanced weather satellite of India configured with improved imaging system and atmospheric sounder as compared to earlier INSAT missions like KALPANA-1 and INSAT-3A. INSAT-3D satellite was launched successfully on 26th July 2013 using an Ariane 5 ECA launch vehicle from Franch, Guiana. It is equipped with a 6-channels Imager and 19-channels atmospheric sounder, which operate in visible to thermal infrared region of the electromagnetic spectrum. Imager operates in VIS (0.55-0.75 µm) and SWIR (1.55-1.70 µm) bands with 1 km spatial resolution and 30 minute temporal resolution, whereas sounder operates in VIS (0.645-0.745 µm) with 10 km resolution and 1 hour temporal resolution. Vicarious calibration was performed to monitor the in orbit degradation of VIS and SWIR bands of imager and VIS band of sounder from INSAT-3D.

This article shows the post-launch vicarious calibration performed using high reflectance target site with uniform and flat terrain (Little Rann of Kutch) for VIS and SWIR channels of imager and VIS channel of sounder from INSAT-3Dto monitor the post-launch changes in the sensor response. The reflectance based approach was used with ground measured surface reflectance and measurements of atmospheric parameters (aerosol optical depth (AOD), total columnar ozone and water vapor). The measured parameters along with pre-launch laboratory measured spectral response function were input to the radiative transfer code for the computation of TOA radiance for both the bands. The 6S radiative transfer code was used to simulate the TOA radiance at the satellite level. The simulated radiance has been compared with the measured radiance from INSAT-3D and the calibration coefficients have been computed for VIS and SWIR of imager and VIS of sounder. The uncertainties due to measurements of surface reflectance, selections of aerosol model, surface anisotropic effect and 6S model uncertainties were computed for the vicarious calibration coefficients of INSAT-3D imager and sounder.

2. Theoretical Background

The calibration and validation of satellite sensor is the process of quantitatively defining and assessing the system response to known and controlled signal inputs, determined by independent means. In remote sensing, a sensor calibration is an important requirement to maintain the quality. For that, regular exercise is a necessity to update the calibration coefficient. Calibration coefficient relates a digital number (DN) observed in an image pixel to its radiance, which is a physical quantity characterizing the radiative property of an earth surface feature represented by the pixel. Prior to satellite launch, sensor is well calibrated in the laboratory and calibration coefficient is computed by measuring sensor response to illumination from a well-defined, standard source of light, traceable to well-known standards such as NIST (National Institute of Standards). The output from the detectors within a sensor in response to a known, well characterized source of radiance, is quantized to a discrete number of gray levels and the calibration relation can be written as:

$$\boldsymbol{L = DN * [(L_{max} - L_{min})/(DN_{max} - DN_{min}) + L_{min}]} \qquad (\mathbf{1})$$

Where, L is the radiance in mW/cm^2/sr/μm and DN is the maximum quantization value, given by 2n, where n is the number of bits used for digitally encoding the data.

A number of factors such as deep space environment, launch stresses, etc. can affect the performance of the sensor onboard a satellite after launch. Sensor optics/detector degradation due to various causes can potentially lead to change in calibration coefficient over time. There is need to monitor these changes (Thome, 2001). Vicarious calibration provides a method to derive sensor calibration coefficient from estimated TOA radiances, which is completely independent from laboratory and on-board calibration.

There are many methods of vicarious calibration, viz., relative calibration, absolute calibration, lunar calibration, etc. That can be used to monitor possible variations in sensor calibration coefficients. Vicarious calibration refers to the process of determining a sensor calibration coefficient using estimated radiance with the ground measurements of reflectance along with atmospheric parameters and satellite sensor observed radiance value of the same surface, at the time of satellite pass. If the instruments used for ground measurements are traceable to NIST or other well-known standards, then the vicarious calibration becomes an absolute calibration. The absolute calibration method has been used for the vicarious calibration of INSAT-3D in this study. The ground measured reflectance is extracted for the corresponding wavelength bands of the sensor and passed through a radiative transfer code to compute TOA radiance. The ground data has been typically averaged using 2x2 moving window over an observational site and computed radiance value using RT model, which are compared with the INSAT-3D observed radiance for the same pixels to derive vicarious calibration coefficient for different bands. The following method has been used for the computation of calibration coefficient.

$$\boldsymbol{L_{esti}/L_{obs} = 1} \qquad \mathbf{(2)}$$

Where, L_{esti} and L_{obs} are estimated and observed radiance at TOA. Any deviation from unity of the ratio between estimated and observed radiance value suggests the requirement of update the calibration coefficient.

3. Test Site and Field Measurements

3.1. *Calibration site*

Attributing to their preferable stability of surface characteristics and atmospheric dynamics, pseudo-invariant sites are commonly used for sensor radiometric calibration, degradation monitoring and inter-comparisons (Chandra et al., 2010; Bouvet et al., 2014) especially for the satellite sensors without on-board calibration facilities. The Committee on Earth Observation Satellites (CEOS) Working group on Calibration and Validation identified several sites around the world (Teillet and Chandra, 2010) based on the selection criteria, such as low probability of atmospheric interruptions, high spatial homogeneity, weak directional effects, flat reflectivity spectrum. Calibration sites are never chosen randomly, and to be adequate they must satisfy a certain number of criteria (Scott et al., 1996; Slater et al., 1996; Slater et al., 1987; Teillet et al., 1997). Based on these criteria, we have selected a desert site in little Rann of Kutch (ROK) (23.51ºN and 71.40º E), Gujarat. This calibration site is extended upto ~50 km square area, presents a flat and homogenous terrain characterized by a high surface reflectance. The site is clay-dominated dry land with different spectral characteristics that have been used for radiometric calibration sites for large footprint sensors. Figure-1(a) and (b) show a false color composite image by Advanced Wide Field Sensor (AWiFS) on board Indian Remote Sensing (IRS) satellite over little ROK and the target site dated 20thFebruary, 2015. Photograph of this site is shown in figure-1(c).

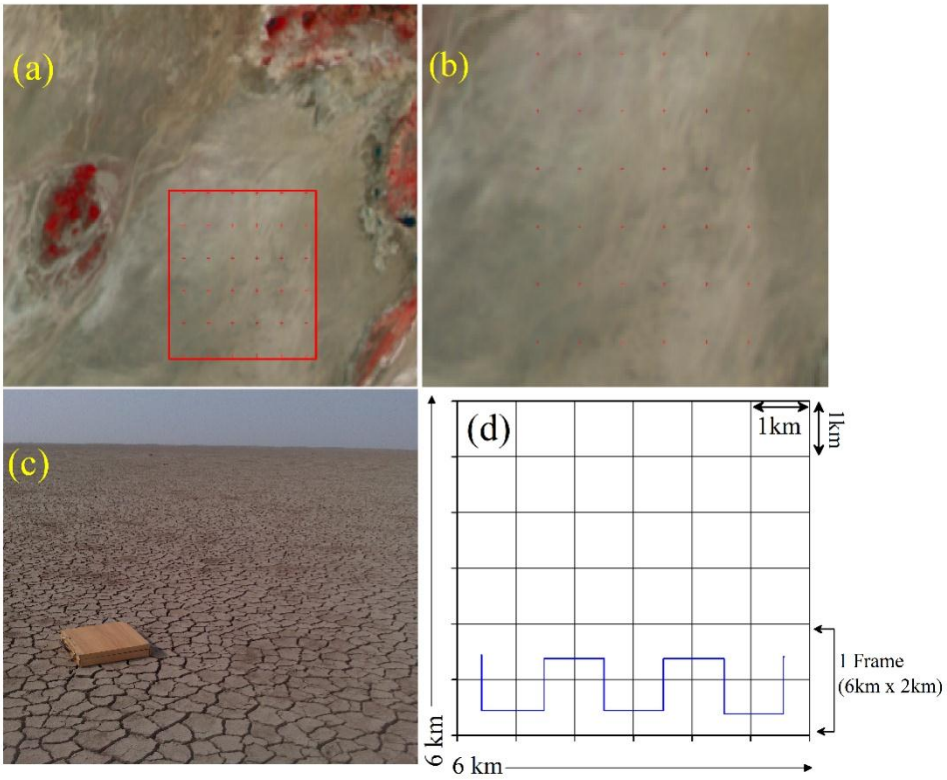

Figure 1:(a) location of calibration site at Little ROK in INSAT-3D image (b) site photograph and (c) data collection methodology.

3.2. *Field campaign*

Measurements of ground reflectance are carried out with a spectroradiometer (FieldSpec 3, Analytical Spectral Devices (ASD), Inc.), which covers the spectral range from 350 to 2500 nm and were made at the center of each 1km grid over the 6 x 6 km region of the calibration site as shown in figure-1(d). The frame-based (1 frame = 6x 6 km^2) approach is used for the data collection. The ground reflectance of 1 frame is measured within ±15 minutes of the satellite overpass. Similarly, the reflectance data on second and third frames is measured in the next consecutive half hours. On ground, data was collected during 10:45 am to 12:15 pm, accordingly triplet (11:00 am, 11:30 am and 12:00 am) of INSAT-3D L1B radiance data are collected. This approach for data collection is more suitable for the vicarious calibration of geostationary satellites like INSAT-3D. Data are collected in zigzag manner within the frame, which is shown in the figure-1(d) in a blue color. Twelve points are covered within 30 minutes (half hour) in a single frame with an interval of 1 km. Total 36 points are covered in a 6 x 6 km2 site within 90 minutes per day. This pattern of measurements is repeated for five clear sky days (17th February 2015, 20th February 2015, 05th March 2015, 17th March 2015 and 20th March 2015). INSAT-3D sounder has a coarse spatial resolution (10 km) and 1 hour temporal resolution, therefore the slight different approach is carried out for the calibration of SND-VIS band. It is difficult to cover 10 km x10 km area for the ground data collection. In view of high spatial uniformity of the site based on the analysis of coefficient of variation (CV) (figure-4: red box (10 km x10 km)) the data are averaged and extrapolated for the larger satellite footprint of INSAT-3D sounder. For the purpose of calibration, daily L1B sounder radiance data for two passes (11:00 am and 12:00 am) are collected, which are collocated with the ground measurements.

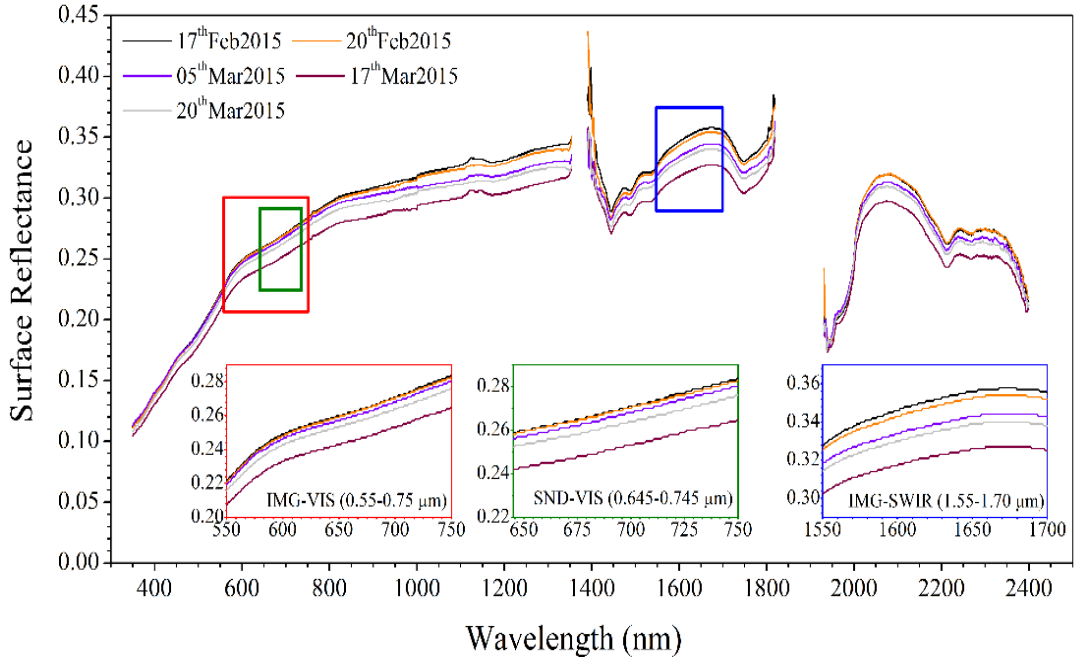

Figure 2: Measured surface reflectance at little ROK for the five clear sky days. Small boxes describe the variation in reflectance for the INSAT-3D bands.

Figure-2 shows the measured surface reflectance over the site for various days along with standard deviation (at 1σ level). Small boxes inside the figure illustrate the variation of reflectance in the INSAT-3D bands. Water vapor absorption at 1380nm and 1800nm are the major reasons for the two gaps in the reflectance curves. The variations in measured reflectance are observed to be 1.7%, 2.3% and 1.9% in IMG-VIS, IMG-SWIR and SND-VIS bands respectively for all the five days, which indicates the uniformity of site. The aerosol optical depth (AOD) measurements were carried out using a multi wavelength Microtops-II sunphotometer (Solar Light Co., USA) at five different wavelengths at 380, 440, 500, 675 and 870 nm, from the solar instantaneous flux measurements with its internal calibration using the Langley method. The Full Width at Half Maximum (FWHM) bandwidth for the 380 nm channel is 2.4±0.4 nm and 10±1.5 for the other channels (Morys et al., 2001). The measured aerosol optical depths are shown in figure-3. High values in the lower wavelength indicates the presence of coarse mode aerosols during 17th - 20th February 2015, whereas loading of accumulation mode particles are observed during other days.

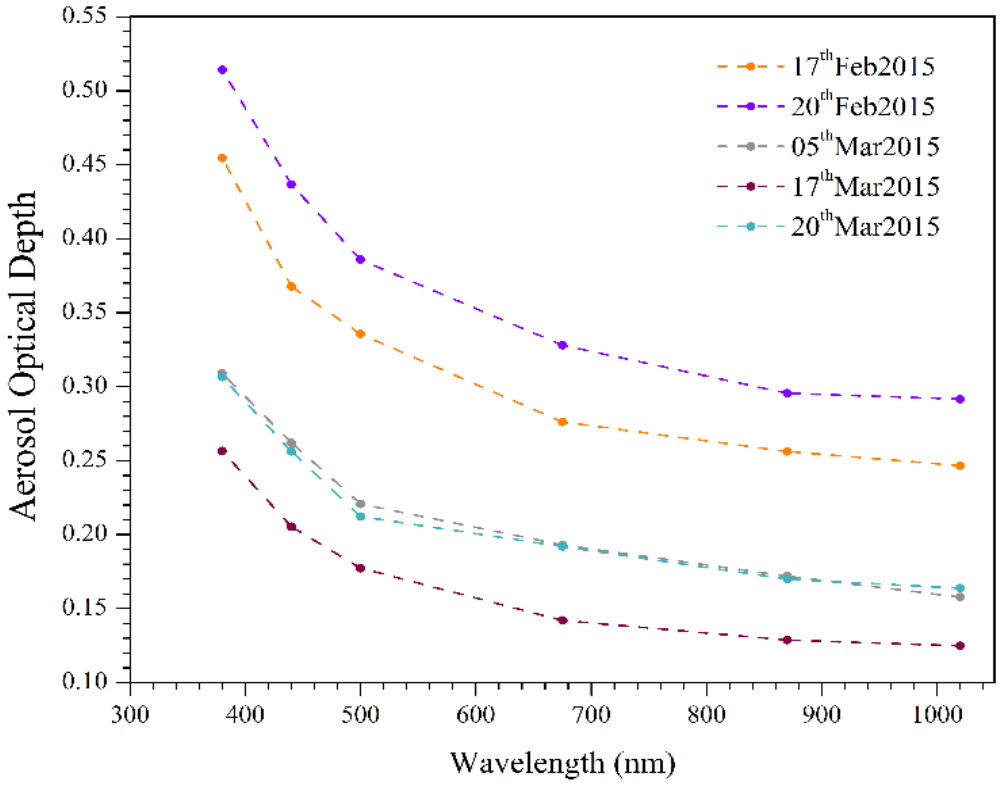

Figure 3: daily mean spectral variation of aerosol optical depth derived by Microtops-II sunphotometer at little ROK on five clear-sky days.

An Ozone monitor, which is capable of measuring the total column ozone (TCO) using three UV channels (305.5, 312.5, 320.0 nm) and the total water vapor content (WVC) using two near-IR channels (940 and 1020 nm) as well as AOD at 1020 nm was also deployed on all the five days.Table-1 contains the daily variation of these parameters over Little ROK for all the five days.

Table 1: Daily mean values of measured atmospheric parameters, i.e. AOD at 500 nm, total columnar ozone and columnar water vapor for all five days over Little ROK.

Date	AOD @ 500 nm	Total ozone (DU)	Water Vapor (g cm^{-2})
17thFeb 2015	0.319±0.012	292.52±5.17	0.96±0.15
20thFeb 2015	0.385±0.031	288.58±5.74	1.09±0.18
05thMar 2015	0.238±0.007	306.35±4.34	1.34±0.15
17thMar 2015	0.146±0.014	307.11±4.20	1.08±0.12
20thMar 2015	0.212±0.008	314.89±3.95	1.49±0.13

3.3. *Site Characteristics*

Radiometric spatial uniformity and temporal stability of targets are the main features to be considered for calibration site selection along with long-term radiometric control of satellite sensor data (Bannari et al., 2005; Cosenfroy et al., 1996; Gu et al., 1990; Rondeaux et al., 1998). The optical characteristics of any target site can vary due to topography variation, surface moisture variation, cracks in the dry surface that trap light, presence of vegetation, non-Lambertian behavior of the surface increasing BRDF effects, as well as meteorological conditions. (Frouin et al., 1987; Scott et al., 1996; Slater et al., 2004; Teillet et al., 1997 ;Thome et al., 2001). Radiometric spatial uniformity and temporal evolution of the little ROK site is ascertained by calculating spatial and temporal Coefficient of Variation (CV) measurements using cloud-free INSAT-3D radiances over the site.

IMG-VIS and IMG-SWIR bands radiance data for 5th March 2015, 11:30 am was analysed to compute CV. CV is defined by the ratio of the standard deviation and the average of the radiances in the box. In order to characterize the variability of the spatial homogeneity of the site, we set a 2 km x 2 km window size with a sampling step of 1 km. Figure-4 illustrates the result obtained using an INSAT-3D image acquired on 5th March 2015 at 11:30 am with the data collected site (6 km x 6 km) in yellow box and extrapolated site (10 km x 10 km) in red box. The CVs are found to be very similar for both the bands of the INSAT-3D imager. The highest values of CV were found to be 5% and 5.5% for IMG-VIS and IMG-SWIR, respectively, on the west side of the calibration site. The mean CV for the data collected site (yellow box) is found to be 2.1% and 1.2% for IMG-VIS and IMG-SWIR. Low variation in radiance over the actual data box (yellow) as well as extrapolated box (Red) indicates spatial radiometric homogeneity of the site and it supports the extrapolation approach for the calibration of SND-VIS.

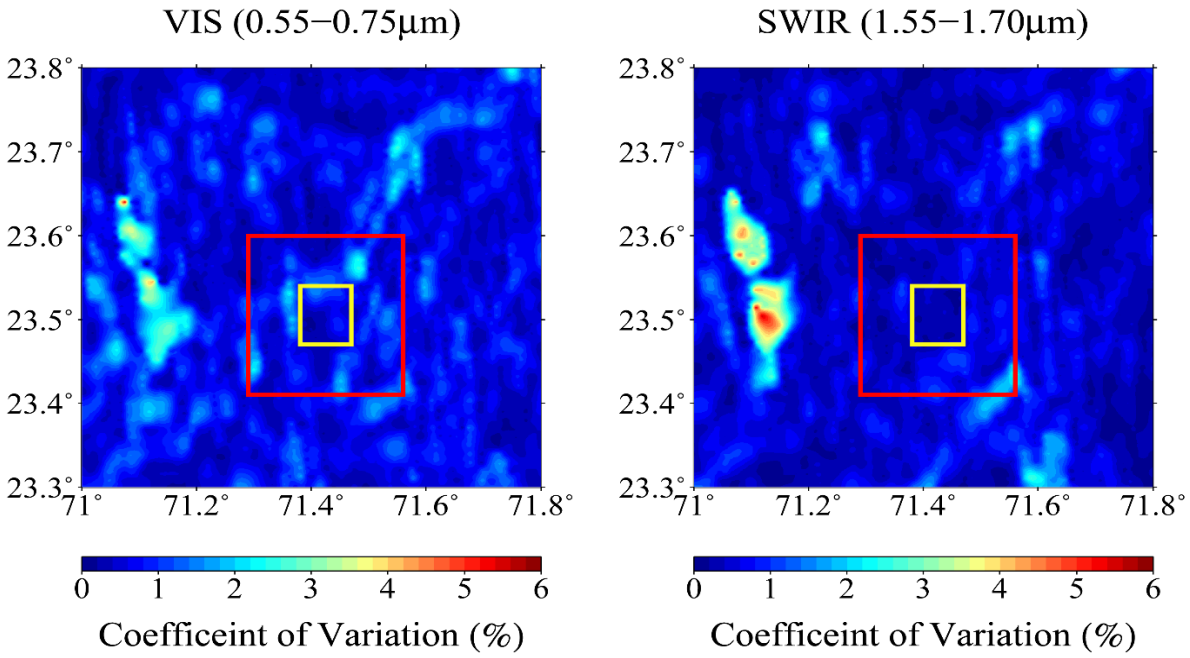

Figure 4: Images of the coefficient of variation calculated using 2km x 2km window in the two bands (IMG-VIS and IMG-SWIR) of a INSAT-3D image acquired over little ROK on 5thMarch 2015 at 11:30 am. Yellow box shows the data collected site (6 km x 6 km) and red box shows the extrapolated site (10 km x10 km).

The temporal CV is evaluated for the five clear sky days using measured reflectance data over the site. Figure-5 indicates how the site surface reflectance has changed over these periods in all three bands (IMG-VIS, IMG-SWIR and SND-VIS) of INSAT-3D. From this figure, it is obvious that the variation of CV is low i.e. 8.1% in IMG-VIS, 6.0% in IMG-SWIR and 7.8% in SND-VIS. These results indicate that these little changes may be caused due to variation in soil moisture resulting from meteorological conditions.

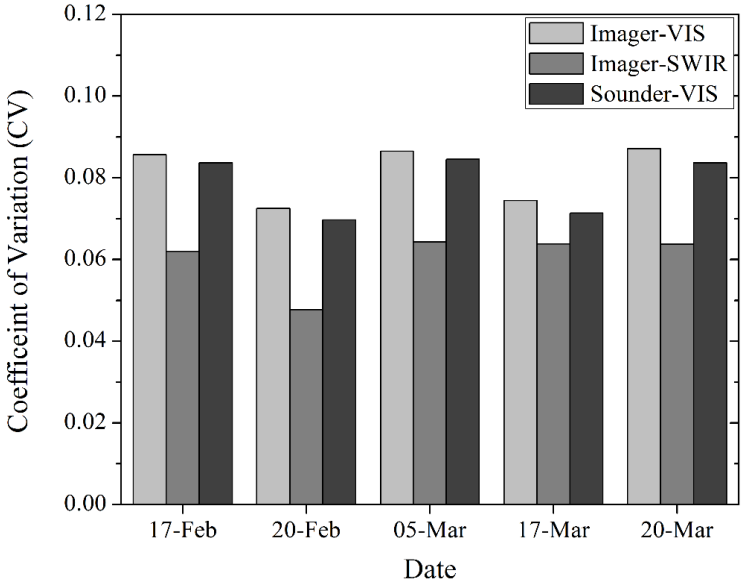

Figure 5: temporal evolution of the three INSAT-3D bands acquired over the little ROK for the study period from 17thFebruary to 20thMarch of 2015.

4. Methodology

Reflectance-based and radiance-based techniques are the most common approaches when in-situ data are used to calibrate satellite sensors (Slater et al., 1987). Reflectance-based technique is used in this study, because it is difficult to maintain the radiometric accuracy of the spectral radiometer that measures the surface radiance at ground in the radiance-based technique.

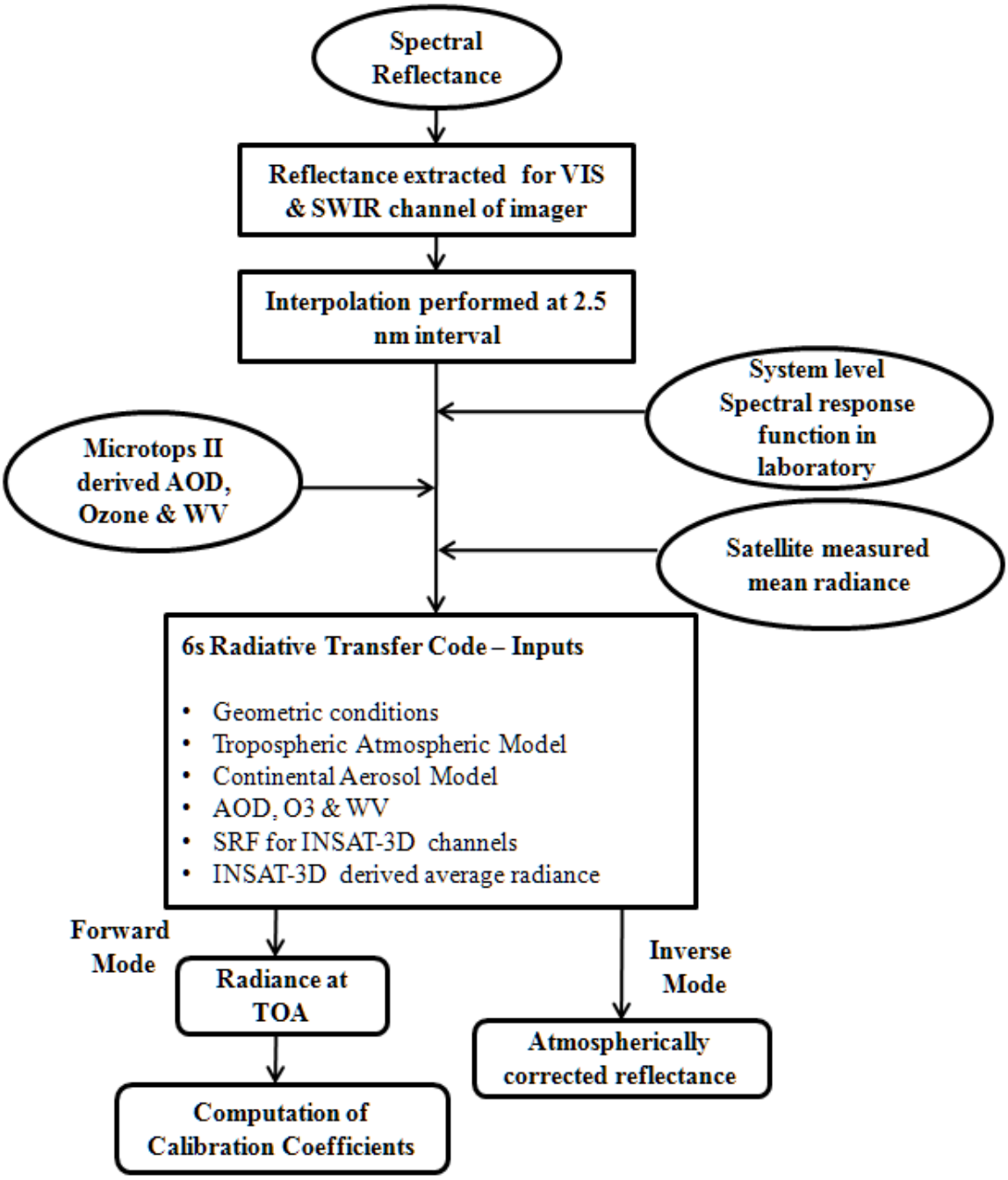

Figure 6: Flow chart for the simulation of TOA radiance and estimation of calibration coefficient.

The reflectance-based technique mainly depends on measured ground surface reflectance. The reflectance is characterized by the ratio of measurement of the site to those of a standard reflectance/Spectralon panel for which the bidirectional reflectance factor is precisely determined. The vicarious radiometric calibration depends on the surface reflectance and radiance from the sun to earth's surface and earth's surface to sensor and atmospheric optical thickness over the calibration site at the time of satellite pass. These measurements are used as an input for radiative transfer (RT) code to simulate the absolute radiances for the required bands at the sensor level. The ground measurements are used to define the spectral directional reflectance of the surface and the spectral optical depth that are used to describe the aerosol and molecular scattering effect in the atmosphere (Gellman et al., 1991) along with this we used columnar water vapor to include the water vapor absorption effect. The detailed values of atmospheric parameters are given in Table-1.We have used 6S RT code to compute the radiance field using ground measurements. 6S RT code predicts the satellite signal at TOA level using ground reflectance measurements and atmospheric measurements of sunphotometer. 6S RT model is a physically based model, which is not specified for particular satellite or test sites because of that 6S RT model is used for this study. In addition, 6S RT model is covered gaseous absorption and scattering by aerosols and molecules. 6S deals better with atmospheric scattering than other RT models (Markham et al., 1992). 6S model was formulated for the atmospheric correction in the short wavelengths. 6S code requires the geometric conditions, including the viewing zenith, viewing azimuth, solar zenith and solar azimuth angles. Viewing zenith and viewing azimuth angles are obtained from INSAT-3D metadata files and solar zenith and solar azimuth angles are calculated using time and location.

Figure-6 describes the detail flow chart to simulate radiance at TOA and vicarious calibration coefficient. The US 62 standard atmosphere profile provides the profiles of water vapor, ozone, pressure and temperature up to 100km, at discrete intervals of 34 layers in the 6S RT model (Vermote et al., 2006).

4.1. *Selection of aerosol model in RT code*

For the selection of optimum aerosol model, we have analysed spectral variation of aerosol optical depth, aerosol size distribution and aerosol type variation using the relation between aerosol optical depth and angstrom exponent (α) (Figure-7).

Figure-7(a) describes the daily mean variation of spectral variation of AOD over calibration site. The higher values in the lower wavelength indicates the presence of coarse mode aerosols during 17th and 20th Feb 2015, whereas the loading of accumulation mode particles are observed during other days. The Angstrom exponent (α) values are calculated in two narrow spectral intervals (340-440nm and 675-870nm) using Microtops-II measured AOD using equation-(3).

$$\boldsymbol{\alpha = -\frac{d \ln \tau_\lambda}{d \ln \lambda} = \frac{\ln(\tau_{\lambda 2}/\tau_{\lambda 1})}{\ln(\lambda_2/\lambda_1)}} \quad \textbf{(3)}$$

The positive or negative values of the difference $\alpha_{340-440} - \alpha_{675-870}$ correspond, in general, to positive or negative values of the curvature of the ln AOD versus ln λ, with the positive

values to suggest dominance of coarse-mode particles and negative values indicates the presence of fine mode particles. In the present study, this relation in figure-7(b) indicates the positive values correspond to the presence of coarse mode particles in most of cases.

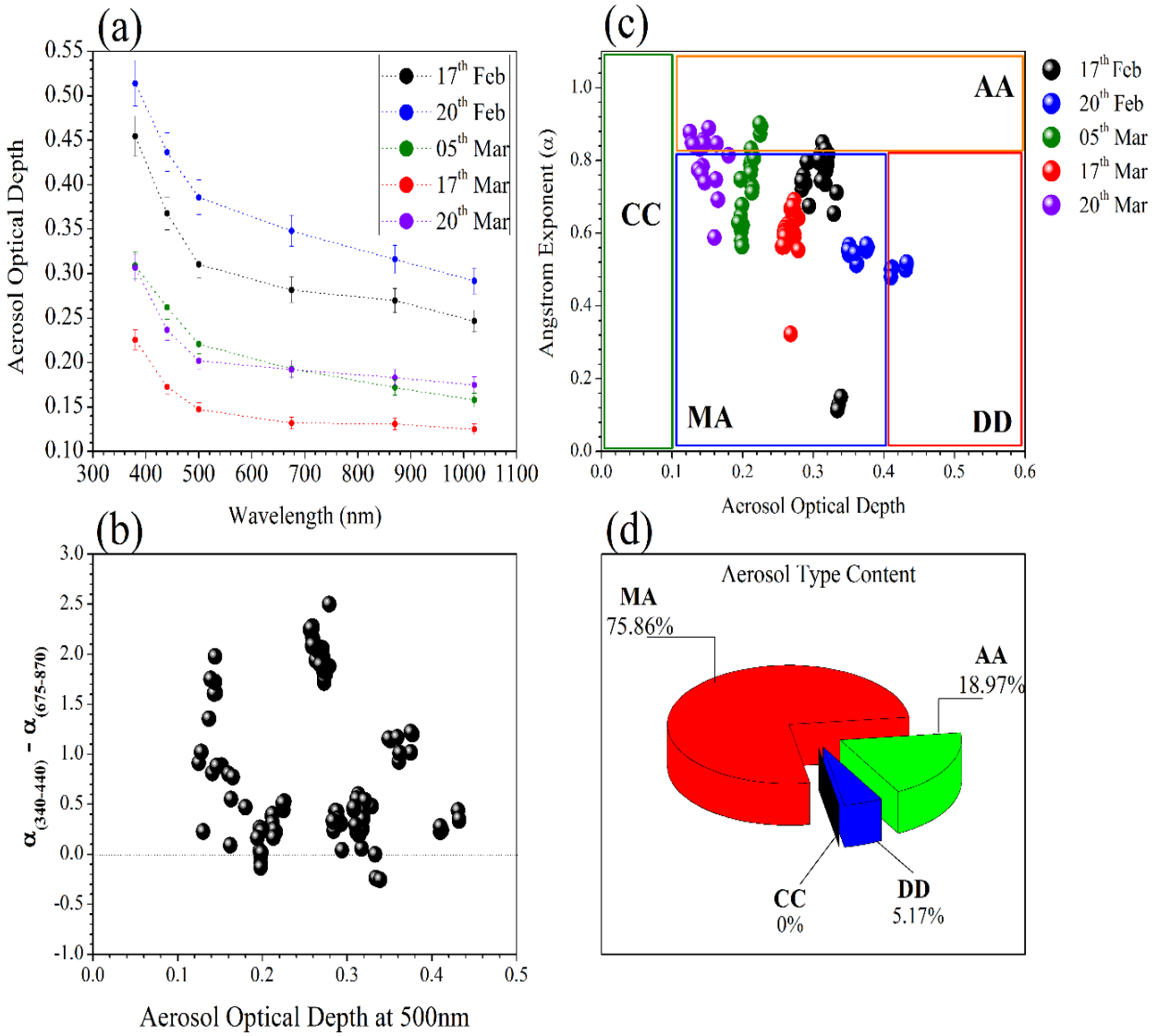

Figure 7: (a) Daily mean variation of spectral AOD, (b) scatter plot of $\alpha_{(340-440)}$ - $\alpha_{(675-870)}$ against AOD at 500 nm, (c) Scatter plot of Angstrom exponent (α(340-870) against AOD at 500nm to discriminate the different aerosol types ((MA-Mixed Aerosol, AA-Anthropogenic Aerosol, DD=Desert Dust and CC= Clean Conditions) and (d) percentage variation of different types of aerosol over Little ROK for the given time-period.

In few cases, the negative values are observed, which may due to the transportation of anthropogenic aerosols from nearby urban areas.We analysed relation between AOD and Angstrom exponent ($\alpha_{440\text{-}870\ nm}$) (Kaskaoutis et al., 2007) because two aerosol properties helps to characterise the aerosol types (Holben et al., 2001). Figure-7(c) illustrates the scatter plot between AOD at 500 nm and $\alpha_{440\text{-}870\ nm}$, to known the aerosol types present over the target site. In this technique, some threshold values are used to discriminate the aerosol types, which may modify with location, aerosol range and aerosol characteristics (Kaskaoutis et al., 2009). In the present study, due to the variation in the range of aerosols, we used slightly

different thresholds than Kaskaoutis et al. (2009) used over Hyderabad. The detection of dust is associated with AOD > 0.4 and α< 0.8, while AOD < 0.1 correspond to clean conditions. The case with AOD > 0.1 associated with α> 0.8 corresponds to anthropogenic aerosols, while AOD between 0.1 and 0.4 associated with α< 0.8 correspond to mixed aerosols. For Little ROK, all aerosols fall under the region of mixed aerosols. Figure-7(d) indicates the percentage variation of different aerosol types over calibration site. It is found that the calibration site experiences 75.86% of mixed type of aerosols along with small loading of 18.97% of anthropogenic aerosols and 5.17% of desert dust, which are probably transport from urban areas and arid regions, respectively. This analysis suggests to use continental aerosol model (a composite with 0.70% of dust like, 0.29% of water-soluble and 0.01% of soot component) in the RT code to simulate the TOA radiance values over calibration site. Continental aerosol model is the basic model over the land site and it is assumed that there is no impact of marine and polluted urban aerosols over Little ROK. The aerosol data with continental aerosol model are used as an input of 6S RT code.

4.2. *Spectral Response Function*

We have used pre-launch laboratory measurements of spectral response function (SRF) of INSAT-3D visible and SWIR channels of Imager and visible channel of sounder as an input to the RT code to compute TOA radiances. The spectral response functions of IMG-VIS, IMG-SWIR and SND-VIS bands are shown in Figure-8.

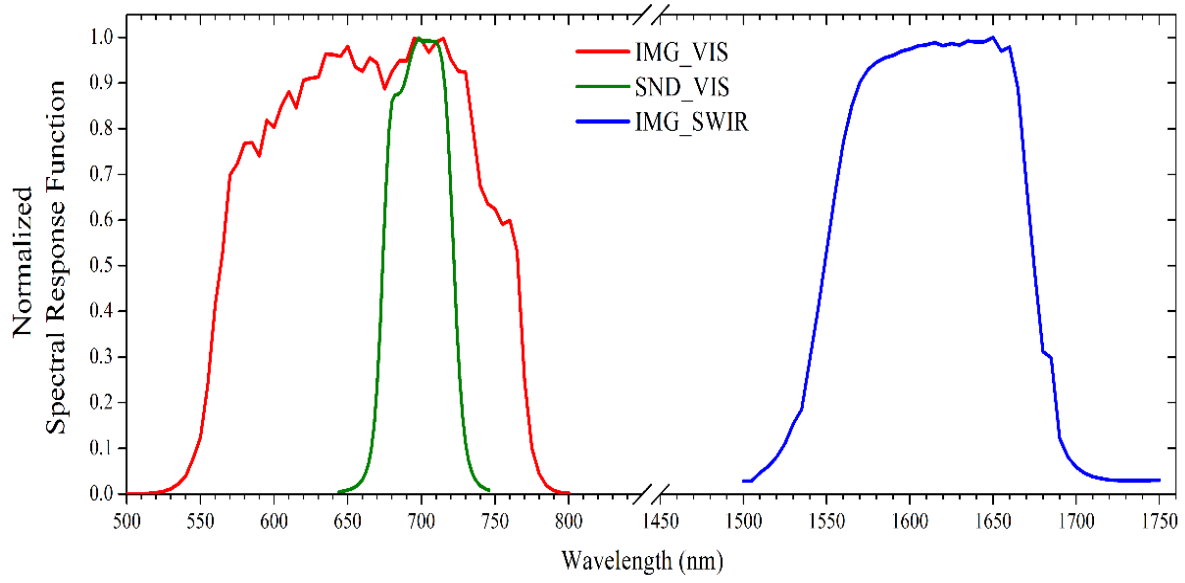

Figure 8: Pre-launch laboratory measurements of spectral response function for IMG-VIS, IMG-SWIR and SND-VIS bands.

As seen in figure, the spectral response functions are slightly asymmetric from the central wavelength. Here due to heterogeneity of shape in the form of Gaussian curve, the concept of FWHM (full width at half maximum) may not be accurate to evaluate the effective bandwidth, beyond which the SRF is effectively zero. There are non-Gaussian SRF methods available to determine effective bandwidth (Palmer 1984). In practice, while there is no significant change in the central wavelength, the use of Palmer method to determine effective

bandwidth of SRF can result in significant difference in values for effective bandwidth as compared to corresponding FWHM bandwidth values (Pandya, 2007). Both the SRF and ground reflectance data are resampled to 2.5 nm intervals using a spline interpolation method. These values with 5% cut-off for each band were used to simulate the radiance using radiative transfer code.

The 6S RT model computes TOA radiance in the forward mode, while it computes atmospherically corrected surface reflectance in the inverse mode. 6S RT model provides an output in the form of TOA radiance, which is divided by the corresponding radiance observed by the INSAT-3D for particular channel to yield calibration coefficients. Similarly, 6S provides atmospherically corrected reflectance as an output for a given radiance in the inverse mode, which are compared with the ground measured reflectance by spectral radiometer.

4.3. *Analysis of BRDF effect*

Surface albedo is related to surface reflectance which depends on the bidirectional reflectance distribution function (BRDF), it reflects how the reflectance depends on solar and view geometries (Nicodemus et al., 1997). Reflectance of light is an anisotropic phenomenon and this anisotropy is very small compared to Lambertian component except surface reflectance from water. The precise computation of surface reflectance requires the anisotropy estimation. The BRDF effect provides a precise computation of uncertainty in reflectance arising due to the neglecting anisotropy. We provided this BRDF effect into 6S using MODIS derived BRDF product (MCD43A1), is used to computes the effects of surface anisotropy on TOA radiance. The high-quality data product MCD43A2 provides high quality three Ross-Li BRDF model parameters (isotropic, volume scattering and geometric optical reflectance terms), which was pixel-wise implemented into 6S RT model to estimates BRDF effect after resampled for 1 km. We used approximately common bands for MODIS and INSAT-3D. MODIS provides BRDF coefficients in the seven MODIS Land bands as well as three broad bands. In which, we used MODIS first broad band (0.4-0.7 μm) for VIS (0.55-0.75 μm) channel of INSAT-3D imager and MODIS SWIR band (1.628-1.652 μm) for SWIR band (1.55-1.70 μm) of INSAT-3D imager. For INSAT-3D sounder, we have used same MODIS first broad band BRDF data. The 6S RT model runs with and without BRDF for the estimation of BRDF effect radiance at top of the atmosphere.

5. Results and Discussions

To carry out the calibration for the IMG-VIS, IMG-SWIR and SND-VIS bands of the INSAT-3D over Little ROK, the 6S simulated TOA radiance was compared with the INSAT-3D radiance for the respected bands.

5.1. *INSAT-3D Imager (VIS & SWIR)*

Figure-9 and 10 describe the combine and daily individuals scatter plots between INSAT-3D measured radiance and 6S simulated radiance for IMG-VIS and IMG-SWIR respectively.

The good statistical agreement was observed between satellite derived radiance and simulated radiance, with R^2 values of 0.99 and 0.99 and with RMSE values of 0.48 and 0.08 for the VIS and SWIR bands respectively. The bias between the satellite derived radiance and 6S simulated radiance are observed very minimal, with the values of 0.40 $Wm^{-2}sr^{-1}\mu m^{-1}$ and 0.07 $Wm^{-2}sr^{-1}\mu m^{-1}$ for VIS and SWIR bands respectively. On average, relative error between the 6S simulated and satellite derived radiances are -0.38% and -0.18%, i.e. INSAT-3D imager overestimates the radiance values by 0.4% and 0.2% in the VIS and SWIR bands. The correlation is found better in IMG-SWIR with respect to IMG-VIS.

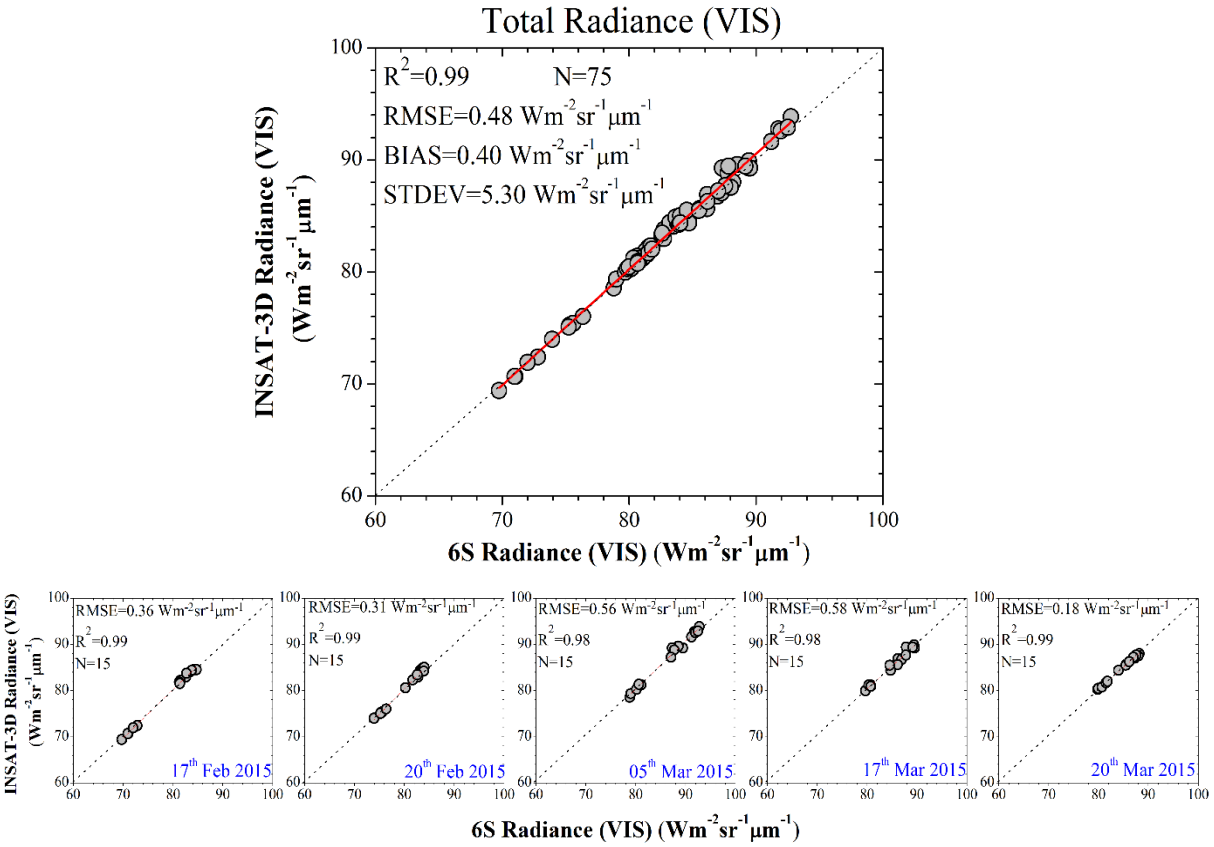

Figure 9: Combine and daily individual comparison of the 6S simulated radiance with INSAT-3D imager radiance for VIS band of INSAT-3D imager over Little Rann of Kutch.

Daily comparison between 6S simulated and INSAT-3D measured radiances indicates the high correlation and it varies within the range of 0.97-0.99 for both IMG-VIS and IMG-SWIR bands of INSAT-3D and the RMSE is found in the range of 0.18-0.56 $Wm^{-2}sr^{-1}\mu m^{-1}$ for VIS and 0.05-0.08 $Wm^{-2}sr^{-1}\mu m^{-1}$ for SWIR bands of INSAT-3D imager.

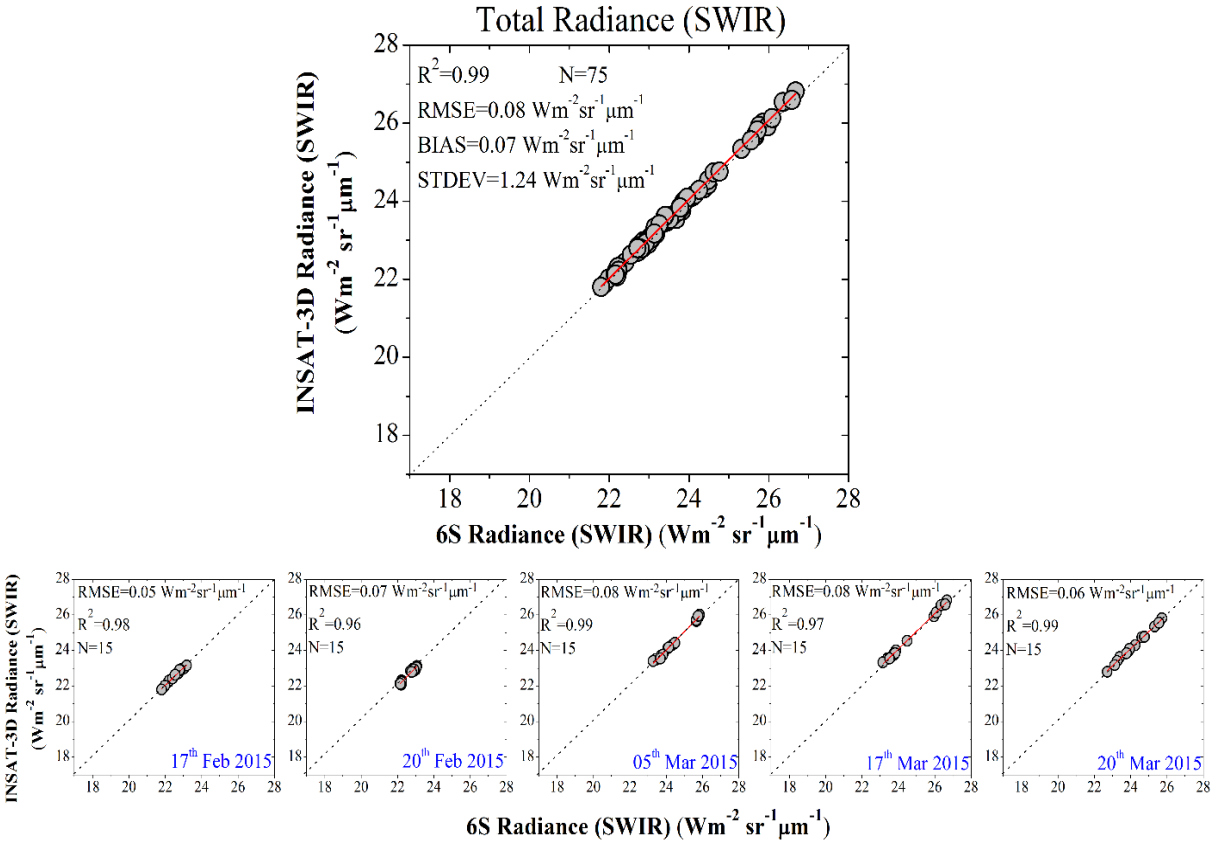

Figure 10 : Combine and daily individual comparison of the 6S simulated radiance with INSAT-3D imager radiance for SWIR band of INSAT-3D imager over Little Rann of Kutch.

Similarly, atmospherically ccorrected surface reflectance is estimated indirectly by using the 6S code in inverse mode. The 6S simulated atmospherically ccorrected surface reflectance is compared with the ground measured reflectance using spectroradiometer is shown in figure-11 and 12 for both VIS and SWIR channels, respectively.The ground measured reflectance from spectral radiometer for INSAT-3D spectral bands (VIS & SWIR) are plotted against the 6S simulated atmospherically corrected reflectance for the Little ROK site. The result of this comparison is shown in the figure-11 and 12. It was observed that the 6S simulated atmospherically corrected reflectance matches well with the ground measured reflectance for both the channels (VIS and SWIR), with R^2 values of 0.98 and 0.98 and RMSE values of 0.0017 and 0.0016 for VIS and SWIR respectively. The agreement is found within ±2% for both the VIS and SWIR spectral bands. The variation in standard deviation is observed 0.013 and 0.015 for VIS and SWIR, which indicates the standard deviations of the measurement sets only and not measurement uncertainties. The small values of standard deviation directly indicates the site variability, which is less than 2% for both the bands. A detail statistical result of the comparison of radiance and reflectance are given in table-2. The result indicates the 6S RT model works well in both forward and inversion mode.

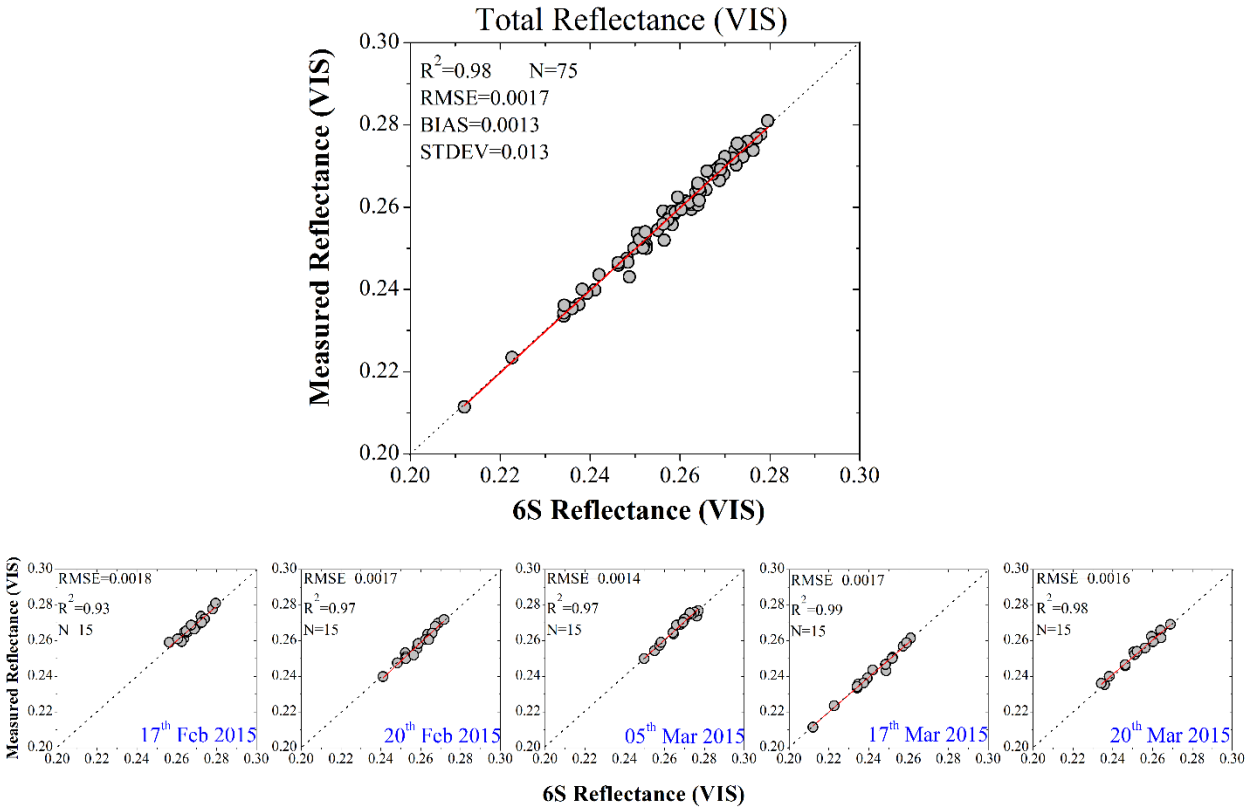

Figure 11: Combine and daily individual comparison of the 6S simulated reflectance with ground measured reflectance for VIS band of INSAT-3D imager over Little Rann of Kutch.

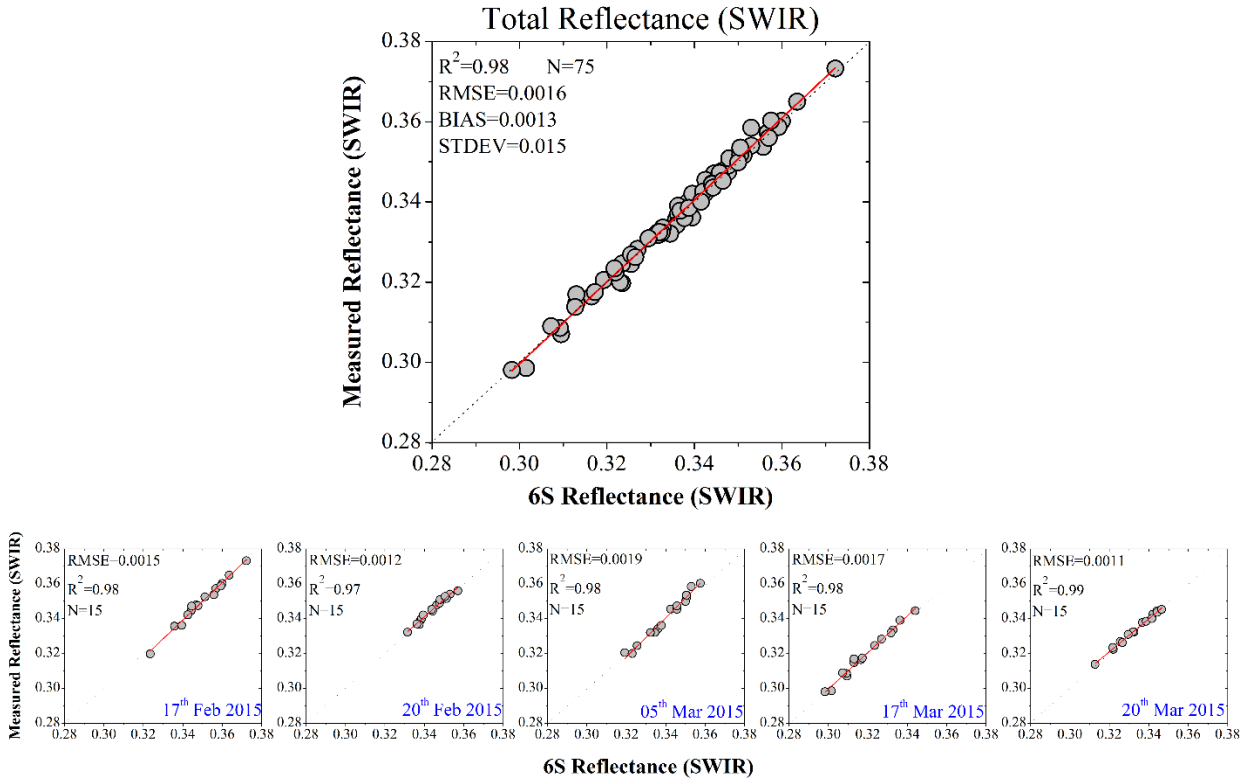

Figure 12: Combine and daily individual comparison of the 6S simulated reflectance with ground measured reflectance for SWIR band of INSAT-3D imager over Little Rann of Kutch.

Table 2: Summary of the statistical results of comparison between INSAT-3D measured radiance and 6S simulated radiance for IMG-VIS, IMG-SWIR and SND-VIS bands over Little ROK site.

	Channels	R^2	Bias ($Wm^{-2}sr^{-1}\mu m^{-1}$)	RMSE ($Wm^{-2}sr^{-1}\mu m^{-1}$)	RE (%)	Standard Deviation ($Wm^{-2}sr^{-1}\mu m^{-1}$)
Radiance	IMG-VIS	0.99	0.46	0.48	-0.38	5.23
	IMG-SWIR	0.99	0.07	0.08	-0.18	1.23
	SND-VIS	0.97	0.46	0.69	-0.13	3.86
Reflectance	IMG-VIS	0.99	0.0013	0.0017	0.07	0.013
	IMG-SWIR	0.99	0.0013	0.0016	-0.12	0.015
	SND-VIS	0.94	0.0015	0.0017	0.23	0.007

It is found that the 6S overestimates the reflectance value by 0.07% in IMG-VIS, whereas it underestimates the reflectance value by 0.12% in IMG-SWIR.

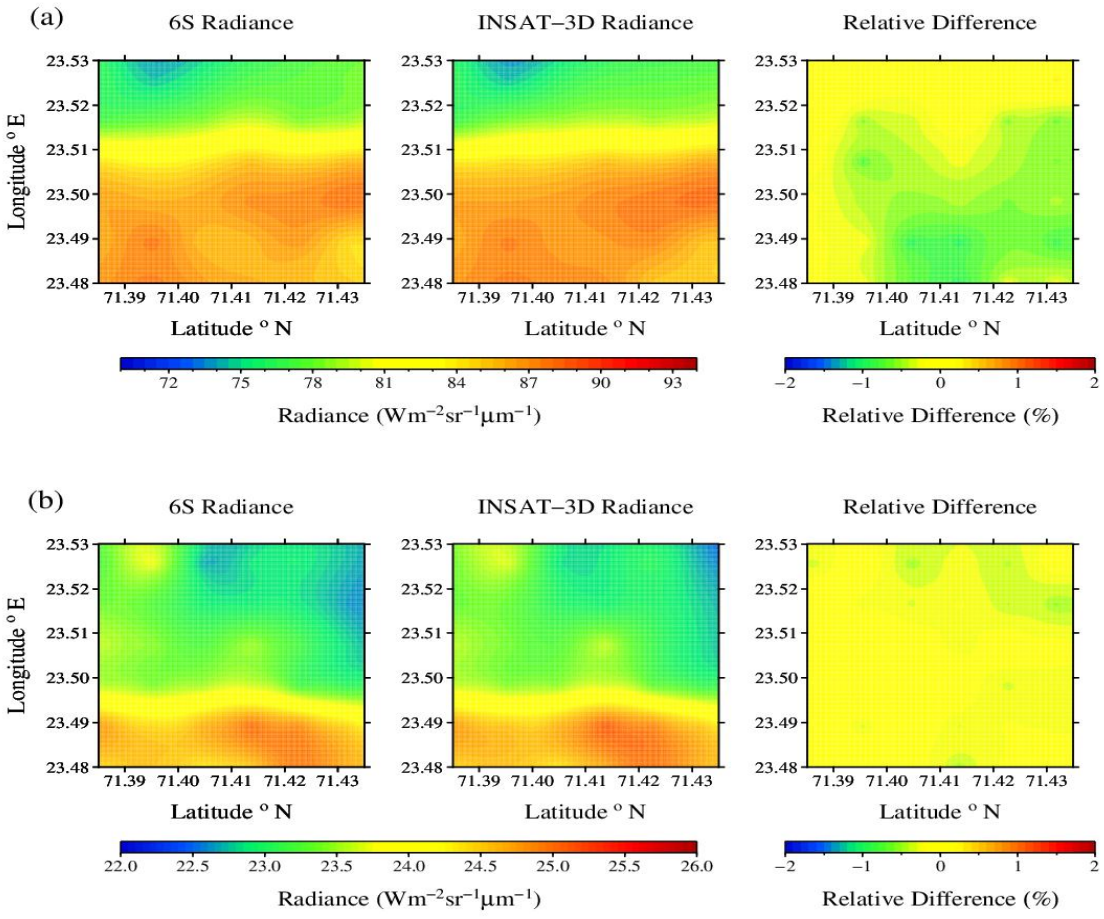

Figure 13: Mean spatial variation of INSAT-3D radiance and 6S simulate radiance along with relative difference for IMG-VIS and IMG-SWIR over Little ROK site.

Figure-13 describes the mean spatial variation of radiance from INSAT-3D and 6S for IMG-VIS and IMG-SWIR along with spatial variation of relative difference between INSAT-3D radiance and 6S radiance over Little ROK. It is observed that the spatial pattern of INSAT-3D derived radiance and 6S simulated radiance is almost similar for both the bands. The impact of temporal variation is clearly observed on the radiance values within the site due to the data collection methodology, which is already discussed in above section. The observed relative difference is very small between INSAT-3D radiance and 6S radiance for both the bands. The variation in terms of relative difference is -1% for IMG-VIS and -0.5% for IMG-SWIR. It means INSAT-3D radiance overestimates the 6S simulated radiance value over both the bands at Little ROK.

5.2. *INSAT-3D Sounder (VIS)*

The calibration of visible channel (0.645-0.745µm) from INSAT-3D sounder (SND-VIS) is also carried out in the present investigation. INSAT-3D sounder measured radiance is compared with 6S simulated radiance over Little ROK.

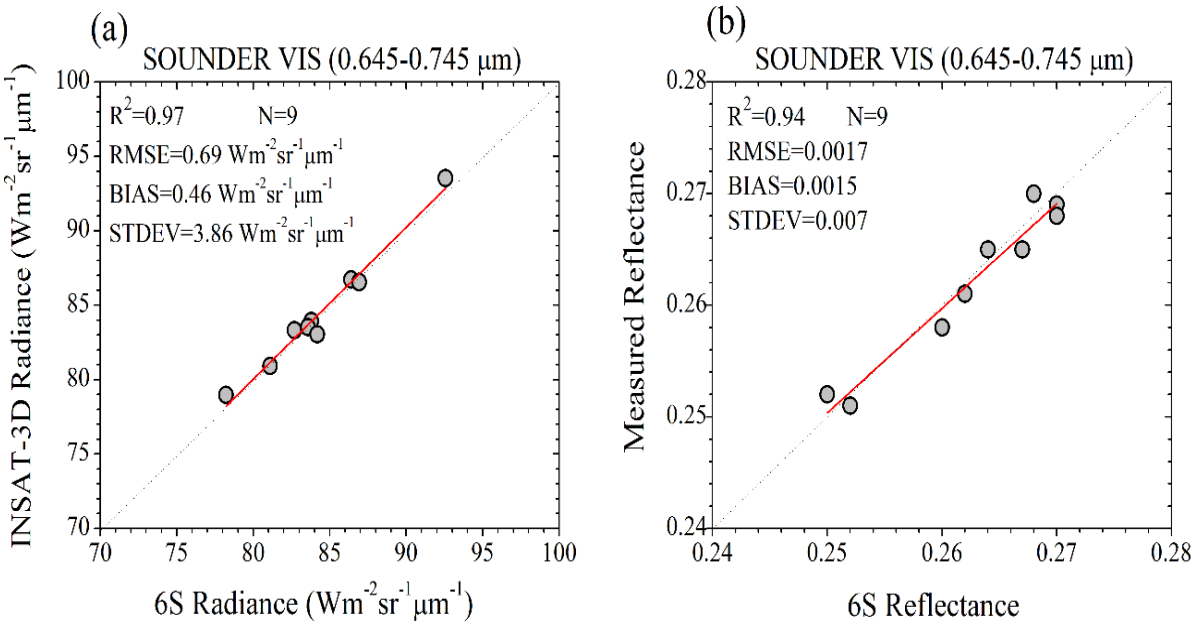

Figure 14: (a) Comparison of the INSAT-3D sounder measured radiance with the 6S simulated radiance for SND-VIS band and (b) Comparison between 6S simulated reflectance and ground measured reflectance for SND-VIS over Little Rann of Kutch.

The SND-VIS has 10 km spatial resolution, therefore the measured reflectance data over the site in 6km x 6km region is interpolated for 10km x 10km region because it is observed that the site is spatially and temporally uniform (figure-4 and 5).With this consideration, the data is interpolated for large spatial resolution and compare with the 6S simulated radiance at TOA. Figure-14(a) illustrates the combine scatter plot of INSAT-3D sounder measured radiance against the 6S simulated radiance and figure-14(b) illustrates the scatter plot between ground measured reflectance and 6S simulated reflectance over calibration site. It is observed that the INSAT-3D sounder measured radiance has a high correlation with 6S simulated radiance with R^2=0.97 and low RMSE = 0.69 $Wm^{-2}sr^{-1}\mu m^{-1}$. The bias between

INSAT-3D sounder and 6S radiance is found to be small 0.46 $Wm^{-2}sr^{-1}\mu m^{-1}$. The relative error is found to be -0.13, it means INSAT-3D measured radiance overestimates the 6S simulated radiance with the value of 0.13%. The comparison between 6S simulated reflectance with the ground measured reflectance shows the good agreement with R^2=0.94 and very low RMSE=0.0017. The RE is observed to be 0.23 indicates the 6S simulate reflectance overestimates the ground measured reflectance with the value of 0.23%.The detail statistics are given in Table-2. The result of calibration of SND-VIS is found better than previously reported result by (Piyushkumar et al., 2014b).The switch-over to the new gain mode 2 for SND-VIS is the main reason for the better calibration result in 2015 (Figure-15).

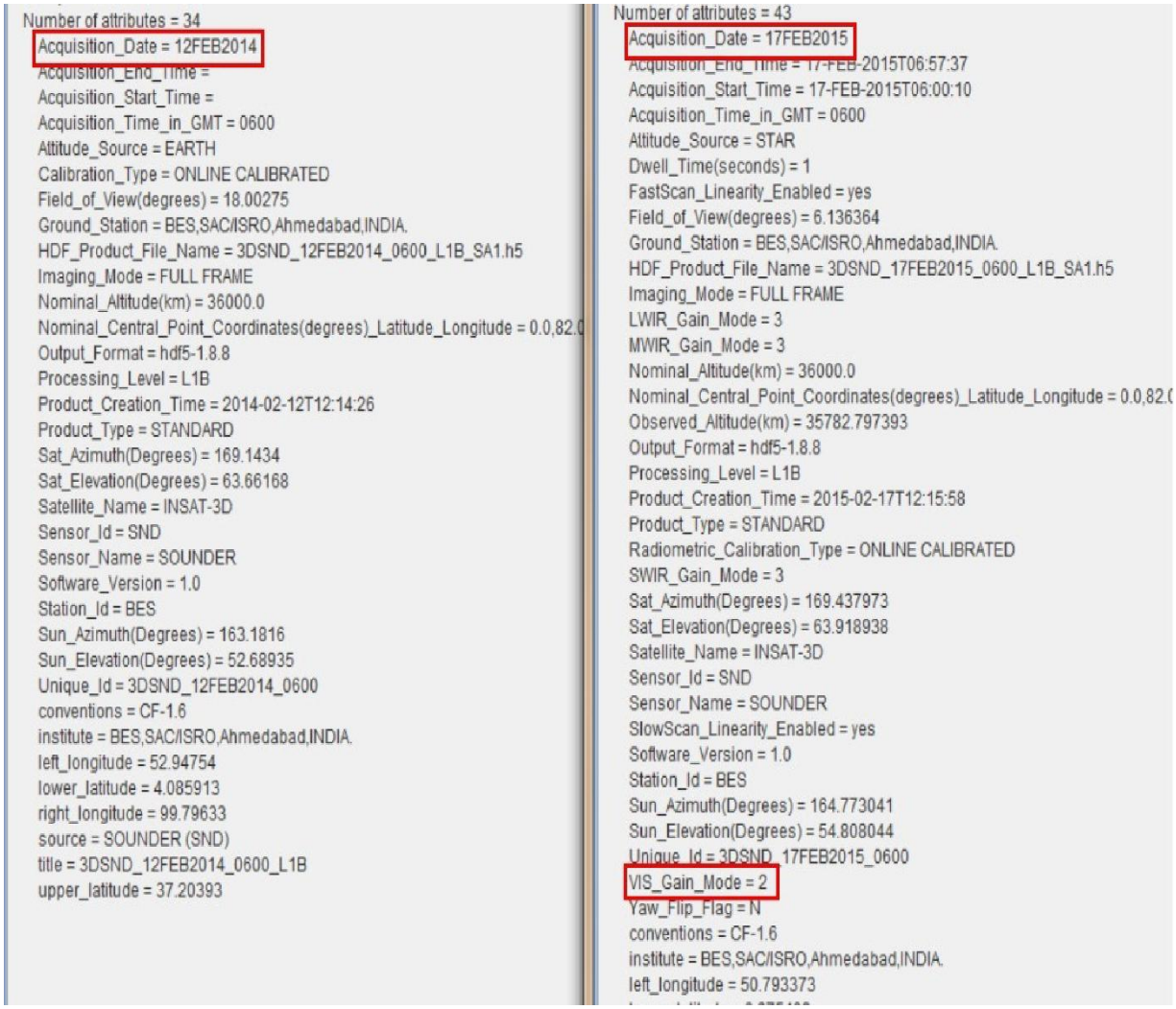

Figure 15: *The change in gain mode for visible channel of INSAT-3D sounder.*

Figure-16 describes the scatter plot between INSAT-3D sounder measured radiance and 6S simulated radiance in (a) previously reported and in (b) present study.

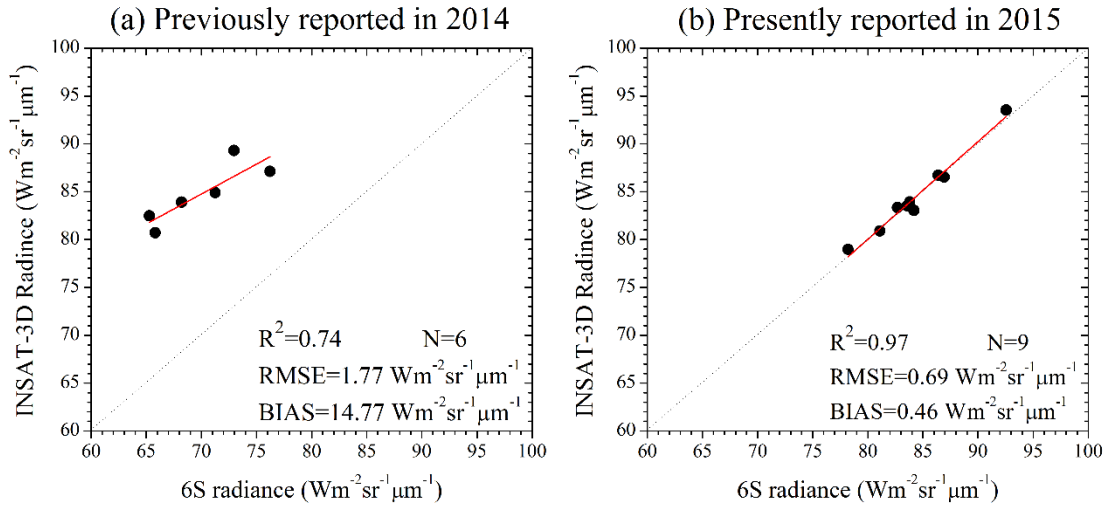

Figure 16: comparison between INSAT-3D sounder and 6S radiance in (a) previous study and in (b) present study.

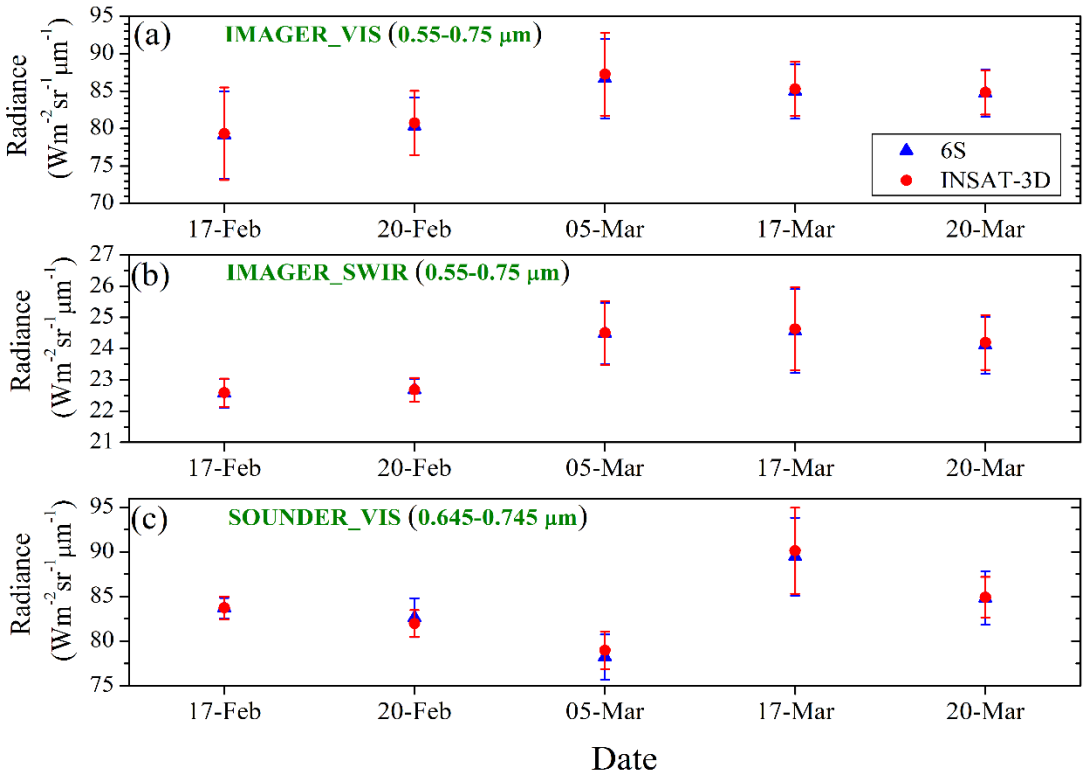

Figure 17: Daily mean variation of INSAT-3D measured and 6S simulated radiance for (a) IMG-VIS, (b) IMG-SWIR and (c) SND-VIS for all five days.

Figure-17 indicates the daily mean variation of INSAT-3D measured radiance and 6S simulated radiance for IMG-VIS, IMG-SWIR and SND-VIS. It is found that the difference between INSAT-3D and 6S simulated radiance is very small for all three channels over calibration site. The mean difference found to be 0.32, 0.04 and 0.12 $Wm^{-2}sr^{-1}\mu m^{-1}$ for IMG-VIS, IMG-SWIR and SND-VIS, respectively. It is found that the INSAT-3D measure radiance overestimates the radiance value for all three channels.

Table 3: The summaries of radiance, reflectance and calibration coefficient for all three channels of the INSAT-3D over calibration site for all five days.

Date	Channels	INSAT-3D Radiance ($Wm^{-2}sr^{-1}\mu m^{-1}$)	6S Simulated Radiance ($Wm^{-2}sr^{-1}\mu m^{-1}$)	Relative Errors in Radiance (%)	Calibration Coefficient	Ground Measured Reflectance	6S simulated atmospherically corrected Reflectance	Relative Errors in Reflectance (%)
17th Feb 2015	IMG-VIS	79.30	79.12	-0.20	0.9982	0.267	0.268	0.11
	IMG-SWIR	22.59	22.56	-0.10	0.9989	0.349	0.349	0.05
	SND-VIS	83.72	83.68	-0.05	0.9995	0.269	0.268	-0.09
20th Feb 2015	IMG-VIS	80.75	80.31	-0.52	0.9947	0.257	0.259	0.45
	IMG-SWIR	22.68	22.67	-0.02	0.9997	0.345	0.344	-0.29
	SND-VIS	81.98	82.63	0.79	1.0079	0.268	0.270	0.18
5nd Mar 2015	IMG-VIS	87.255	86.66	-0.66	0.9933	0.267	0.266	-0.23
	IMG-SWIR	24.51	24.48	-0.10	0.9990	0.341	0.340	-0.13
	SND-VIS	78.97	78.22	-0.94	0.9905	0.265	0.267	1.19
17th Mar 2015	IMG-VIS	85.28	84.96	-0.39	0.9961	0.241	0.242	0.25
	IMG-SWIR	24.63	24.56	-0.30	0.9969	0.319	0.318	-0.15
	SND-VIS	90.13	89.47	-0.71	0.9928	0.265	0.266	-0.20
20th Mar 2015	IMG-VIS	84.82	84.72	-0.12	0.9987	0.253	0.252	-0.24
	IMG-SWIR	24.20	24.11	-0.37	0.9962	0.333	0.332	-0.09
	SND-VIS	84.93	84.81	-0.15	0.9984	0.265	0.264	0.58

5.3. *Vicarious Calibration Coefficient*

Table-3 describes the mean TOA radiance, surface reflectance and vicarious calibration coefficient derived from measurements at the Little ROK site over all five days. From table-3, the mean values of simulated and satellite observed radiance are highly comparable throughout the three bands of INSAT-3D. The differences between simulated and observed radiance are very small and which is due to the intrinsic variability and meteorological variabilities of the sites.

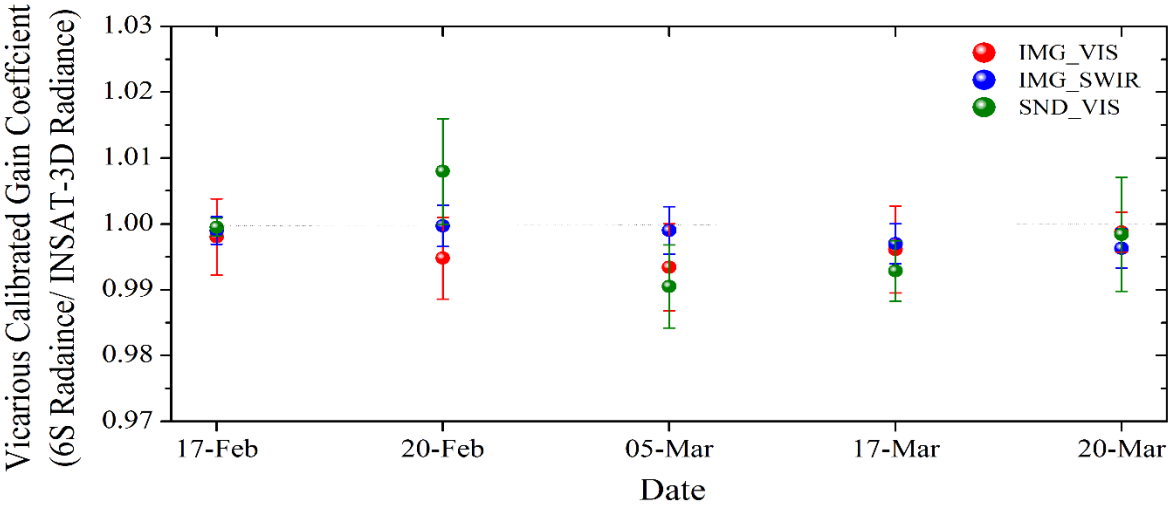

Figure 18: Daily variation of estimated vicarious calibration coefficients for all five days.

The vicarious calibration coefficient is the ratio of 6S simulated radiance and satellite observed radiance. For an ideal case, if there is no degradation in the sensor during launch and ground and atmosphere are absolutely characterized and have an accurate RT code, simulated TOA radiance should precisely match with satellite observed radiance. It means the ratio of simulated to observe radiance should be unity. In practice it is not possible, there are uncertainties in field reflectance and atmospheric measurements, modeling uncertainties in the RT code. Figure-18 describes the ratio of the TOA radiance simulated using ground measured data to the INSAT-3D derived radiance for each channel and each day. The vicarious calibration coefficient data for INSAT-3D imager describes very minor changes in the calibration of INSAT-3D for all three channels and the change is slightly more in SND-VIS channel with respect to others. The standard deviation of the calibration coefficient is less than 2% for each channel in Figure-18. The mean calibration coefficients are found to be 0.996, 0.998 and 0.997 for IMG-VIS, IMG-SWIR and SND-VIS, respectively. This may supports the observed radiance has the simulated radiance versus offset radiance. This study aims towards our methodology and indicating that the errors (< 5%) lie within the radiometric uncertainty. The result indicates the good stability of previously derived calibration coefficients for IMG-VIS and IMG-SWIR by Patel et al., (2014c).

6. Uncertainty Analysis

The simulated TOA radiance is depend on many variables (i.e. atmospheric parameters, geometry, surface reflectance measurements, sensor response function, radiative transfer code etc.). For this study many factors are affecting the accuracy of the calibration

and improving the uncertainty, which is difficult to quantify all these factors. These uncertainties are given together with total error for both wavelength regions.

(a) (σ_a): Reflectance measurements for the radiance simulation at TOA. The uncertainty associated with reflectance measurements is due to angular and spectral variation, which arises to an uncertainty of 1%. This is the combined error directly associated with ASD field spectral radiometer.

(b) (σ_b): The uncertainty in the reflectance measurement is due to variation in the surface characteristics over the region. This uncertainty estimated by calculating the standard error for each band. The average relative errors arise of 1.7% 2.3% and 1.9% for IMG-VIS, IMG-SWIR and SND-VIS data.

(c) (σ_c): The uncertainty arises due to 6S RT model. The error in the 6S RT model is figured out to be approximately 2%.

(d) (σ_d): The selection of the aerosol model in the 6S RT model arises an uncertainty (Gao et al., 2009). This model creates an error because the Little ROK site has a mixed kind of aerosol type. There is a mixture of continental, desert and urban models. For error estimation we calculated new calibration coefficients with the desert and urban models in 6S RT model (see table-4).

Table 4: The new calibration coefficient using desert and urban aerosols models in the 6S RT model along with relative errors arise using these models.

Spectral Channels	Calibration Coefficients (Desert aerosols model)	Relative Errors	Calibration Coefficients (Urban aerosols model)	Relative Errors
IMG-VIS	0.985	0.29%	0.983	0.48%
IMG-SWIR	0.978	0.31%	0.976	0.51%
SND-VIS	0.981	0.30%	0.979	0.50%

(e) (σ_e): The Bi-directional Reflectance Distribution Function (BRDF) effect is adding an uncertainty into calibration coefficient, which is one of the important steps in calibration. Table-5 represents the daily mean uncertainty due to the BRDF effect in both the bands. We used mean values of BRDF effect of all three days for uncertainty estimation (IMG-VIS = 0.518%,IMG-SWIR = 0.88% and SND-VIS=0.78%).

Table 5: The uncertainties were introduced by BRDF effect for both the channels.

Channels	17th Feb	20th Feb	5th Mar	17th Mar	20th Mar
IMG-VIS	0.53%	0.55%	0.47%	0.51%	0.53%
IMG-SWIR	0.9%	0.89%	0.87%	0.88%	0.86%
SND-VIS	0.75%	0.81%	0.77%	0.79%	0.78%

The total uncertainty is estimated using following equation:

$$\boldsymbol{Total\ Uncertainty}\ (\boldsymbol{\sigma}) = \sqrt{\boldsymbol{\sigma_a^2 + \sigma_b^2 + \sigma_c^2 + \sigma_d^2 + \sigma_e^2}} \qquad (\mathbf{4})$$

From the above analysis, the total uncertainty is found 2.87%, 3.43% and 3.05% for IMG-VIS,IMG-SWIR and SND-VIS bands of INSAT-3D, respectively.

7. Conclusion

In this study, post-lunch calibration was carried out for the VIS and SWIR bands of INSAT-3D imager and VIS band of INSAT-3D sounder over the Little ROK site. The TOA radiance was simulated by 6S RT model using ground measurements.
The other conclusions based on this study are summarized below:

(1) The 6S simulated radiance are in good agreement with the INSAT-3D measured radiance for all three bands over Little ROK.
(2) The close agreement was observed between simulated and satellite measured TOA radiance. The mean vicarious calibration coefficients for the INSAT-3D vary between 1.3% for VIS and 1.9% for SWIR for all three dates over Little ROK site.
(3) There are well statistical agreement was observed between ground measured reflectance and 6S simulated atmospherically corrected reflectance in the inverse mode.
(4) The spatial and temporal variability of site is quantified by the variation of mean reflectance and coefficient of variation. The mean reflectance varies 1.7%, 2.3% and 1.9%for IMG-VIS, IMG-SWIR and SND-VIS bands, where the CV was found to be lesser for the Little ROK site (1%-2%) in all three bands of INSAT-3D.
(5) Uncertainty in TOA radiance due to selection of aerosol model is much less. The uncertainty is found to be ~0.3% for desert model and ~0.5% for urban model with respect to continental model.
(6) Uncertainty due to BRDF effect is estimated using MODIS BRDF products, which was found to be 0.518%, 0.88% and 0.78% for IMG-VIS, IMG-SWIR and SND-VIS.
(7) The present study concludes that Little ROK site is the preferred site for post-launch calibration due to high degree of homogenous in nature, which helps to derive precise vicarious calibration coefficients.
(8) The observed degradation in the VIS and SWIR channel of INSAT-3D imager and VIS channel of INSAT-3D sounder is very minor. The mean value of vicarious calibration coefficients are 0.996, 0.998 and 0.997 for IMG-VIS, IMG-SWIR and SND-VIS, respectively.
(9) The previously derived calibration coefficients produced by Patel et al., (2014c) are valid till date and the noted values are found to be consistent, which indicate good calibration stability of visible and SWIR channels of INSAT-3D imager.

Acknowledgement

The authors gratefully acknowledge the encouragement received from Director, SAC for carrying out the present research work. Valuable suggestions received from Deputy Director, EPSA are also gratefully acknowledged.

References

1. Biggar S.F., Dinguirard M.C., Gellman D. I., Henry P., Jackson R. D., Moran M.S., Slater P. N., Proc. SPIE, 1991, 1493, 155-162.
2. Biggar S.F., Slater P.N., and Gellman D. I., "Uncertainties in the in-flight calibration of sensors with reference to measured ground sites in the 0.4 to 1.1 _m range," *Remote Sens. Environ.*, vol. 48, pp. 242–252, 1994.
3. Bruegge, C.J., Duval, V.G., Chrien, N.L., Korechoff, R.P., Gaitley, B.J.and Hochberg, E.B., (1998), MISR prelaunch instrument calibration and characterization results. IEEE Transactions on Geoscience and Remote Sensing, 36, pp. 1186–1198.
4. Bruegge, C.J., Stiegman, A.E., Rainen, R.A. and Springsteen, A.W., (1993), Use of Spectralon as a diffuse reflectance standard for in-flight calibration of earth-orbiting sensors. Optical Engineering, 32, pp. 805–814.
5. Gellman D. I., Biggar S.F., Slater P.N., and Bruegge C.J., "Calibrated intercepts for solar radiometers used in remote sensor calibration," *Proc. SPIE*, vol. 1493, pp. 19–24, 1991.
6. Gellman D. I., Biggar S.F., Dinguirard M.C., Henry P.J., Moran M.S., Thome, K.J., Slater, P.N., Proc. SPIE, 1993, 1938, 118-125.
7. Holben, B.N., Tanr, D., Smirnov, A., Eck, T.F., Slutsker, I., Abuhassan, N., Newcomb, W.W., Schafer, J.S., Chatenet, B., Lavenu, F., Kaufman, Y.J., Vande Castle, J., Setzer, A., Markham, B., Clark, D., Frouin, R., Halthore, R., Karneli, A., O'Neill, N.T., Pietras, C., Pinker, R.T., Voss, K., Zibordi, G., (2001). An emerging ground-based aerosol climatology: Aerosol Optical Depth from AERONET. J. Geophys. Res. 106, 12 067–12 097.
8. Kaskaoutis, D.G., Kambezidis, H.D., Hatzianastassiou, N., Kosmopoulos, P., Badarinath, K.V.S., (2007). Aerosol climatology: on the discrimination of the aerosol types over four AERONET sites. Atmos. Chem. Phys. Discuss. 7, 6357–6411.
9. Kaskaoutis, D.G., Badarinath, K.V.S., Kharol, S.K., Sharma, A.R., Kambezidis, H.D., (2009). Variations in the aerosol optical properties and types over the tropical urban site of Hyderabad, India. J. Geophys. Res. 114, D22204. doi:10.1029/2009JD012423
10. Markham, B. L., Halthore, R. N., & Goetz, S. J. (1992). Surface reflectance retrieval from satellite and aircraft sensors: results of sensor and algorithm comparison during FIFE. Journal of Geophysical Research, 97 (D17± 18), 785± 795.
11. Nicodemus F.E., Richmond J.C., Hsia J.J., Ginsberg I.W., and Limperis T., Geometrical considerations and nomenclature for reflectance , Natl. Bur. Stand. Rep., NBS MN-160, 52 pp., 1977.
12. Piyushkumar, P. N., Hiren, B. and Shukla, A. K. (2014a). Vicarious radiometric calibration of INSAT-3D (IMGER) VIS and SWIR channels over Little Rann of Kutch, scientific report, SAC/EPSA/ADVG/CVD/CAL-VAL/03/2014.

13. Piyushkumar, P. N., Hiren, B. and Shukla, A. K. (2014b). Vicarious calibration of VIS channel of INSAT-3D sounder and validation of INSAT-3D derived ozone products, scientific report, SAC/EPSA/ADVG/CVD/CAL-VAL/SR/06/2014.
14. Piyushkumar, P., Hiren, B. and Shukla, A. K. (2014c). Absolute vicarious calibration of recently launched Indian meteorological satellite: INSAT-3D Imager, Vol. XL-8, 2014, ISPRS Technical Commission VIII Symposium, 09-12 December 2014, Hyderabad, India, doi:10.5194/isprsarchives-XL-8-291-2014.
15. Rao, C.R.N., (2001), Implementation of the Post-Launch Vicarious Calibration of the GOES Imager Visible Channel (Camp Springs, MD: NOAA Satellite and Information Services (NOAA/NESDIS)).
16. Slater P.N., Biggar S.F., Holm R.G., Jackson R.D., Mao Y., Moran M.S., Palmer J.M., and Yuan B., "Reflectance- and radiance-based methods for the in-flight absolute calibration of multispectral sensors," *Remote Sens. Environ.*, vol. 22, pp. 11–37, 1987.
17. Slater P.N., Biggar S.F., Palmer J.M., and Thome K.J., "Unified approach to pre- and in-flight satellite sensor absolute radiometric calibration," *Proc. SPIE*, vol. 2583, pp. 130–141, 1995.
18. Thome K., Markham B., Barker J., Slater P., and Biggar S., "Radiometric calibration of Landsat," *Photogramm. Eng. Remote Sensing.*, vol. 63, pp. 853–858, 1997.
19. Thome, K., Schiller, K.S., Conel, J., Arai, K. and Tsuchida, S., (1998), Results of the 1997 Earth Observing System Vicarious Calibration joint campaign at Lunar Lake Playa, Nevada (USA). Metrologia, 35, pp. 631–638.
20. Vermote, E., D. Tanre, J. L. Deuze, M. Herman, J. J. Morcrette, and S. Y. Kotchenova. (2006). *Second Simulation of Satellite Signal in the Satellite Spectrum* (*6S*). 6S User Guide Version 3, University of Maryland.
21. Yang, J., Gong, P., Fu, R., Zhang, M., Chen, J., Liang, S., et al. (2013). The role of satellite remote sensing in climate change studies. Nature Climate Change, 3,875–883.